Review

Relevance of polynomial matrix decompositions to broadband blind signal separation

Soydan Redif[a,*], Stephan Weiss[b,1], John G. McWhirter[c]

[a] Department of Electrical & Electronic Engineering, European University of Lefke, Lefke, North Cyprus
[b] Department of Electronic & Electrical Engineering, University of Strathclyde, Glasgow G11XW, Scotland
[c] Cardiff University, Cardiff CF24 3AA, Wales, UK

ARTICLE INFO

ABSTRACT

The polynomial matrix EVD (PEVD) is an extension of the conventional eigenvalue decomposition (EVD) to polynomial matrices. The purpose of this article is to provide a review of the theoretical foundations of the PEVD and to highlight practical applications in the area of broadband blind source separation (BSS). Based on basic definitions of polynomial matrix terminology such as parahermitian and paraunitary matrices, strong decorrelation and spectral majorisation, the PEVD and its theoretical foundations will be briefly outlined. The paper then focuses on the applicability of the PEVD and broadband subspace techniques — enabled by the diagonalisation and spectral majorisation capabilities of PEVD algorithms — to define broadband BSS solutions that generalise well-known narrowband techniques based on the EVD. This is achieved through the analysis of new results from three exemplar broadband BSS applications — underwater acoustics, radar clutter suppression, and domain-weighted broadband beamforming — and their comparison with classical broadband methods.

1. Introduction

Over the last decade, algorithms that extend the eigenvalue decomposition (EVD) to the realm of polynomial matrices have had a growing impact on signal processing theory and practice, mainly because they can be used to solve generalisations of narrowband problems typically addressed by the EVD, including subspace decomposition. The extension of EVD to parahermitian (PH) polynomial matrices, referred to as polynomial matrix EVD (PEVD), gives an immediate broadband generalisation of the concepts of signal and noise subspaces, and hence subspace decompositions. Just as principal component analysis (PCA) based on the EVD is fundamental to most narrowband BSS formulations, the PEVD can be a powerful tool for broadband or convolutive blind source separation (BSS).

The classical approach to narrowband BSS begins by exploiting second-order statistics to generate uncorrelated sequences from narrowband, instantaneously mixed signals by performing principal component analysis (PCA) [1,2]. PCA is usually obtained through matrix factorisation by means of a unitary matrix decomposition, such as the singular value (SVD) or eigenvalue decomposition (EVD) [3,4]. To complete the BSS process, a "hidden" rotation matrix is determined via on higher-order statistics (HOS), which permutes entries to achieve

spectral coherence across frequency bins. With little or no prior knowledge and minimal assumptions, a BSS method can often be used to extract a wanted signal from among interference signals. However, the wanted signal is in no way accentuated by these underlying assumptions.

Incorporation of a priori knowledge of the signals into the BSS problem can be formulated in the framework of signal decompositions and matrix factorisations, and address statistical dependence, periodicity, spectral shape, time coherence or smoothness [5–8]. The goal often is to estimate a reduced coordinate space, which provides a more accurate physical representation of the sources or mixing parameters.

The above signal decompositions are based on an instantaneous mixing model, where the propagation of signals from sources to the array is modelled as a scalar mixing matrix. However, in many important applications such as broadband array processing, convolutive mixing — or a matrix of finite impulse response (FIR) filters — must be used instead. The transfer function of such a matrix of FIR filters forms a polynomial matrix, which can accurately model effects such as multipath propagation, or the lag-dependent correlation between different broadband sensor signals. SVD- or EVD-based decompositions generally can only decorrelate instantaneously, i.e., only for zero lag. Following convolutive mixing, strong decorrelation

---

[9] eliminates correlation for all lag values, and can be achieved using a well-designed matrix of FIR filters.

In the past, broadband BSS has been addressed by performing narrowband BSS at each frequency bin simultaneously, through application of the discrete Fourier transform (DFT) — commonly referred to as independent frequency bin (IFB) processing. However, coherence restoration is required after BSS via permutation matrices applied in every bin [10,11]. An alternative is to adopt coherent signal subspace-related methods, which generally require some prior knowledge of signals, such as direction and fractional bandwidth, to coherently combine covariance matrices across different bins in order to create an approximately narrowband problem [12–14].

The formulation and decomposition of polynomial matrices presents an alternative to these classical broadband BSS approaches. Polynomial matrices have been used for many years, e.g., in the area of control [15] or broadband subspace decomposition and adaptive sensor arrays [16–18]. Various polynomial matrix factorisations have been addressed, such as the Smith–Macmillan form [19], or polynomial matrix factors that are paraunitary (PU) or lossless [20–33]. Typically, the filter is chosen to optimise a specific objective function for a known input power spectral density (PSD), such as coding gain [9,20,23,31,32] for subband coding.

The space–time covariance matrix derived from broadband sensor data includes auto- and cross-correlation terms, whose symmetries create the specific form of a parahermitian (PH) polynomial matrix. The PEVD of such a PH matrix was proposed in [16,25,26], and leads to a factorisation where a diagonal PH matrix containing the polynomial eigenvalues is pre- and post-multiplied by a PU matrix, or lossless, filter bank. The existence of such a factorisation based on FIR PU matrices is not ascertained [19], but suggested that it exists at least in good approximation [34].

The polynomial eigenvalues of a PEVD represent the power spectral densities of the strongly decorrelated signals. Depending on the PEVD algorithm (discussed below), the eigenvalues can be ordered akin to the singular values of the SVD at every frequency. The ordering of the spectra in this way is called spectral majorisation [9,26], and is useful in a number of applications.

An initial iterative scheme to approximate the PEVD, the second order sequential best rotation (SBR2) algorithm [26], has triggered similar or related efforts [28–33,35–40]. SBR2 has been proven to converge [26,31], and found to approximate the ideal PEVD very closely [34]. A coding-gain based version of SBR2 (SBR2C) was shown to offer improved convergence in [31].

More recently, the sequential matrix decomposition (SMD) and maximum-element (ME-SMD) algorithms [33] have shown superior convergence due to their advanced energy transfer ability, as compared to other iterative algorithms. The multiple-shift variant of the ME-SMD in [36] has shown marked improvement in convergence speed compared to SMD.

The SMD and SBR2 algorithms have been successfully applied to a number of broadband extensions of narrowband problems, traditionally addressed by the EVD, including, e.g., broadband array processing [41–47], channel coding [48], broadband communications [49], spectral factorisation [50], convolutive BSS [42,46], and the design of FIR PU filter banks for subband coding [31,32]. The recent parallelisation of SBR2 in [35], for field programmable gate arrays, has enabled application of SBR2 to real-time problems using embedded processing [51].

The advantage of polynomial matrix decompositions over IFB processing lies in the natural ability of broadband decomposition algorithms to preserve and exploit the coherence of signals.

As a particular example of applying the PEVD to convolutive BSS with prior knowledge, in [42] a broadband extension to the narrowband semi-blind signal approach in [52] has been performed. The broadband equivalent method used some prior information about the direction of sources acquired by a broadband array was embedded to

achieve an enhanced separation of sources. This can be combined with other broadband approaches, such as polynomial MUSIC [44,45], to estimate the prior knowledge that can then be passed to the BSS problem.

The aim of this paper is twofold: (i) provide an overview of polynomial matrix factorisation and (ii) discuss applications in the area of broadband BSS. In Section 2, the PEVD and related fundamental concepts, such as paraunitarity, strong decorrelation and spectral majorisation, are introduced. In Sections 3 and 4, we present solutions and new results to three important problems via a PEVD-based broadband beamformer and domain-weighted PEVD. The results are compared to classical methods, which contrast the natural ability of broadband subspace decomposition algorithms to preserve and exploit the coherence of signals. Lastly, conclusions are drawn in Section 5.

2. Polynomial matrix eigenvalue decomposition

2.1. Notation

In this paper matrices and vectors are represented by bold upper-case and bold lowercase characters, e.g., $\mathbf{X}$ and $\mathbf{x}$, respectively. An element of $\mathbf{X}$ is denoted by x_{jk}. Complex conjugation, matrix transposition and Hermitian transposition are indicated by the superscripts *, T and H, respectively. A $p \times p$ (complex-valued) Hermitian matrix $\mathbf{R} \in \mathbb{C}^{p \times p}$ has the property $\mathbf{R} = \mathbf{R}^H$; a unitary matrix $\mathbf{U} \in \mathbb{C}^{p \times p}$ has the property $\mathbf{U}^H\mathbf{U} = \mathbf{U}\mathbf{U}^H = \mathbf{I}_p$, where $\mathbf{I}_p$ is the $p \times p$ identity matrix.

Polynomial matrices are polynomials with matrix-valued coefficients, or matrices with polynomial elements [15,19]. An $n \times q$ polynomial matrix in the indeterminate variable z^{-1} is denoted by

$$A(z) = \sum_{\tau=t_1}^{t_2} \mathbf{A}[\tau]z^{-\tau}, \tag{1}$$

where $a_{ij}(z) = \sum_{\tau=t_1}^{t_2} a_{ij}[\tau]z^{-\tau}$, $t_1 \le t_2$, $\tau \in \mathbb{Z}$ and $a_{ij}[\tau] \in \mathbb{C}$, is an element of $\mathbf{A}[\tau]$. Hence, coefficient matrices of $A(z)$ can be written as $\mathbf{A}[t_1], ..., \mathbf{A}[t_2]$; e.g., the coefficient matrix of lag zero (lag-zero coefficient matrix) is denoted $\mathbf{A}[0]$. Note that the effective order of $A(z)$ is $t_2 - t_1$. A transform pair as in (1) is abbreviated as $A(z) \bullet\!\!-\!\!\circ \mathbf{A}[\tau]$. Also note that parentheses express dependency on continuous variables, while square brackets denote dependency on discrete variables.

2.2. Space–time covariance matrix

It is well-known that instantaneous spatial correlation, i.e., correlation between pairs of signals sampled at the same instant in time, can be removed using the EVD and SVD [4]. Therefore, the SVD (or EVD) can be used to decorrelate instantaneous mixtures, e.g., for the case of narrowband sensor arrays. However, convolutively mixed signals, or signals derived from a broadband sensor array, cannot be decorrelated in this way. The sensor-weight values required to correct for the time delay between sensors are different for different frequencies. Frequency dependent weights can be realised using FIR filters, which form a frequency dependent response for each sensor signal in order to compensate the phase difference for the different frequency components. The sensors thus sample the propagating wave field in both space and time.

Hence, in order to express the signals at the sensors, we modify the well-known instantaneous-mixing (or narrowband) model to take account of this process

$$\mathbf{x}[t] = \mathbf{A}[t] * \mathbf{s}[t] + \boldsymbol{\eta}[t], \tag{2}$$

where the asterisk denotes multi-input multi-output (MIMO) convolution [51], $\mathbf{A}[\tau] \circ\!\!-\!\!\bullet A(z)$ is the $p \times q$ mixing matrix of FIR filters $a_{ij}[t]$ and $\mathbf{s}[t] \in \mathbb{C}^q$ and $\boldsymbol{\eta}[t]$ represent independent source and noise signals.

The signals $\mathbf{x}[t]$ will generally be correlated over multiple time lags,

so that the space–time covariance matrix,

$$\mathbf{R}[\tau] = \mathcal{E}\{\mathbf{x}[t]\mathbf{x}^{\mathrm{H}}[t - \tau]\} \in \mathbb{C}^{p \times p}, \tag{3}$$

will generally not be diagonal for all τ, where $\mathcal{E}\{\cdot\}$ denotes the expectation operator. It follows that the cross-spectral density (CSD) matrix, $\mathbf{R}(z) \bullet\!\!-\!\!\circ \mathbf{R}[\tau]$, will also not be diagonal. It can be shown that the CSD matrices of the signal and noise sources are both diagonal because of the independence assumption.

The matrix $\mathbf{R}(z)|_{z=e^{j\Omega}} = \mathbf{R}(e^{j\Omega}) \in \mathbb{C}^{p \times p}$ is Hermitian for all normalised frequencies Ω. Equivalently, we say that the polynomial matrix is parahermitian (PH): $\widetilde{\mathbf{R}}(z) = \mathbf{R}(z) \; \forall z$, where $\widetilde{\mathbf{R}}(z)$ is the paraconjugate of $\mathbf{R}(z)$, i.e., $\widetilde{\mathbf{R}}(z) = \mathbf{R}_*^{\mathrm{T}}(z^{-1})$, and the asterisk denotes complex conjugation of the polynomial coefficients. Note that in the case where $\mathbf{R}(z)$ is of order zero, paraconjugation becomes Hermitian conjugate.

2.3. Polynomial eigenvalues and eigenvectors

In order to decompose the space–time covariance matrix $\mathbf{R}[\tau]$ of (3) in an analogous fashion to the EVD, the role of the EVD unitary matrix [3,4] must be generalised to the polynomial case. To this end, we require a matrix of filters that are lossless: the total power at every frequency is invariant under the transformation. In linear system theory, this type of system is termed a lossless (all-pass) MIMO system [19]. In terms of polynomial matrices, we need a polynomial matrix to be paraunitary (PU). A polynomial matrix is PU iff $H(z)\widetilde{H}(z) = \widetilde{H}(z)H(z) = \mathbf{I}_p$. Equivalently, $H(z)|_{z=e^{j\Omega}} = \mathbf{H}(e^{j\Omega}) \in \mathbb{C}^{p \times p}$ is unitary $\forall \Omega$, which is clearly energy preserving.

For PU matrices $H(z)$ comprising FIR components, the CSD matrix $\mathbf{R}(z)$ can be decomposed as

$$\Sigma(z) \approx H(z)\mathbf{R}(z)\widetilde{H}(z) = \mathrm{diag}\{\sigma_1(z), \sigma_2(z)\ldots\sigma_p(z)\}, \tag{4}$$

where $\sigma_i(z) \bullet\!\!-\!\!\circ \sigma_i[\tau] = \mathcal{E}\{v_i[t]v_i^*[t - \tau]\}$ are the polynomial eigenvalues of $\mathbf{R}(z)$ and the row of $H(z)$ are the "polynomial eigenvectors" of $\mathbf{R}(z)$. Here $v_i[t]$ denote the signals after transformation by $H(z)$.

We use the approximation sign in (4) to indicate that a PEVD factorisation with FIR PU matrices does not necessarily exist; however, Icart and Comon have shown that a very close approximation is possible with arbitrarily large filter orders [34].

The decomposition in (4) represents a generalisation of the EVD to polynomial matrices, namely polynomial matrix EVD (or PEVD). Note that (4) becomes the EVD of a Hermitian matrix for a zero-order $\mathbf{R}(z)$. The notion of a unitary matrix for scalar matrices is extended to that of a PU matrix.

2.4. Strong decorrelation and spectral majorisation

A set of signals $v_i[t]$ has the strong (total) decorrelation property if the signals are decorrelated for all relative time delays — not just at the same time instant for all signals. That is,

$$\mathcal{E}\{v_i[t]v_j[t - \tau]\} = 0, \tag{5}$$

for all t, τ and $i \neq j$ [9]. If the diagonalising PU matrix $\mathbf{H}[\tau]$ of (4) is applied to the signals $\mathbf{x}[t]$ in (2), i.e.,

$$\mathbf{v}[t] = \mathbf{H}[t] * \mathbf{x}[t], \tag{6}$$

then the transformed signals will be strongly decorrelated. In other words, if $H(z)$ diagonalises the PH matrix $\mathbf{R}(z)$, it will also impose strong decorrelation.

The problem of finding a PU matrix with the aim of imposing strong decorrelation occurs in many other applications besides convolutive BSS, such as in the design of filter banks for subband coding [9,31,32].

The PU matrix $H(z)$ in (4) can be designed such that the set of power spectra $\{\sigma_i(e^{j\Omega})\}$, where $\sigma_i(e^{j\Omega}) = \sigma_i(z)|_{z=e^{j\Omega}}$, of the transformed signals $\mathbf{v}(z)$ satisfies *spectral majorisation* [9]:

$$\sigma_1(e^{j\Omega}) \geq \sigma_2(e^{j\Omega}) \geq \cdots \geq \sigma_p(e^{j\Omega}), \; \forall \Omega \in [-\pi, \pi). \tag{7}$$
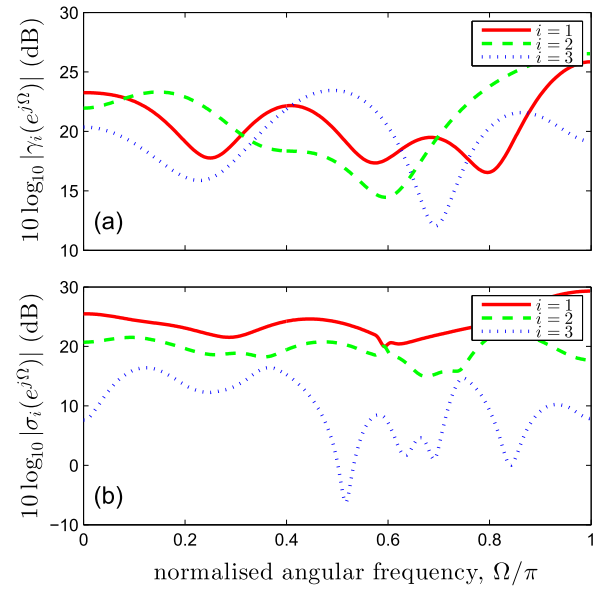

Fig. 1. Example of spectral majorisation: signal spectra that (a) do not have and (b) have the spectral majorisation property.

Note that (7) is the polynomial analogue to an ordered EVD [3] or the way singular values are ordered by the SVD.

As an example of spectral majorisation via a PU matrix, consider the power spectra, $\gamma_i(e^{j\Omega})$, for three arbitrary signals, shown in Fig. 1(a). These signals clearly do not satisfy the spectral majorisation property in (7). However, processing these signals with an appropriately designed PU matrix yields the spectrally majorised PSDs, $\sigma_i(e^{j\Omega})$, as shown in Fig. 1(b).

In addition, a PU matrix $H(z)$ can be found so that the transformed signals satisfy *energy compaction*: $\sigma_i[0] \geq \sigma_{i+1}[0]$, where $\sigma_i[0] = \mathcal{E}\{|v_i[t]|^2\}$. Thus, the total spectral power in the first transformed signal $v_1(z)$ is maximised, and the total spectral power in each of the remaining signals is maximised successively. This property implies spectral majorisation (in (7)), and is directly analogous to the singular value ordering for the narrowband case.

Spectral majorisation is a very important property in applications such as broadband beamforming and BSS. This is because spectrally majorised signals tend to have most of the related (correlated) signal energy focused in as few channels as possible [26,41]. This property is very useful when the aim is to identify the signal subspace, as in broadband subspace decomposition.

In Sections 3 and 4, we show how the spectral majorisation and energy compaction properties are of paramount importance in achieving broadband BSS for signals derived from sensor arrays.

It can be shown that the total input signal power, for all frequencies, is invariant under a PU transformation [19]. A PU operation cannot attenuate or amplify the power across channels, it can only redistribute it, thus maintaining the physical significance of the power of output signals.

2.5. Approximating the PEVD

All PEVD algorithms presented in the literature to date are suboptimal since they can only approximate the PEVD. They can also be viewed as blind methods in the sense that they use minimal a priori information about the signal sources. The only information used by these algorithms is the space–time covariance matrix $\mathbf{R}[\tau]$ in (3), which, in practice, is estimated using a finite window of N samples of the input signal $\mathbf{x}[t]$. The accuracy of this estimate is therefore crucial for the accuracy of the PEVD. Assuming zero-mean signals, an estimate of the space–time covariance matrix in (3) is given by

$$\widehat{\mathbf{R}}[\tau] \triangleq \frac{1}{N} \sum_{t=0}^{N-1} \mathbf{x}[t]\mathbf{x}^{\mathrm{H}}[\tau - t] \tag{8}$$

and

$$\widehat{\mathbf{R}}(z) \triangleq \sum_{\tau=-W}^{W} \widehat{\mathbf{R}}[\tau] z^{-\tau} \tag{9}$$

is the estimated CSD matrix.

It is assumed that $\widehat{\mathbf{R}}[\tau] \cong 0$ for $|\tau| > W$ [26]; for broadband signals, $\widehat{\mathbf{R}}[\tau]$ is negligibly small, if $|\tau|$ is large compared to the coherence time. In practice, W is often measured experimentally. We also assume that $\mathbf{x}[t] = 0$ for values of t outside the sample interval. It can be shown that the polynomial matrix $\widehat{\mathbf{R}}(z)$ is PH by construction.

Iterative PEVD algorithms such as those of the SBR2 [25,26,31,37] and SMD families [33,36] may be used to find a PU matrix $\mathbf{H}(z)$ such that

$$\widetilde{\mathbf{H}}(z)\widehat{\mathbf{R}}(z)\mathbf{H}(z) = \widehat{\mathbf{D}}(z), \tag{10}$$

where $\widehat{\mathbf{D}}(z)$ is approximately diagonal; more specifically,

$$\widehat{\mathbf{D}}(z) \approx \mathrm{diag}\{d_1(z), d_2(z)\dots d_p(z)\}, \tag{11}$$

where $d_i(z) \bullet\!\!-\!\!\circ d_i[\tau] \cong \mathcal{E}\{v_i[t]v_i^*[t - \tau]\}$. The lossless FIR filter $\mathbf{H}(z)$ then produces an output $\mathbf{v}[t]$ according to (6). It can be shown that, to a good approximation, the signals $\mathbf{v}[t]$ are strongly decorrelated.

In Sections 3.3 and 4, we demonstrate, via simulation results, the effectiveness of suboptimal PEVD algorithms as a solution to broadband BSS.

3. Broadband BSS using second-order statistics

Consider the problem of recovering a broadband desired signal by a sensor array in the presence of a broadband interference signal and noise, as illustrated for the two-sources, two-sensors case in Fig. 2. The received broadband signals, $\mathbf{x}[t]$, may be described as convolutive mixtures of the source signals, $\mathbf{s}[t]$, as in (2).

A broadband beamformer can be used to steer the beam created by a sensor array toward the desired signal. Range-bearing plots can then be produced using the beamformer output, from which the target's location can be gathered.

3.1. Broadband conventional beamforming

The broadband conventional beamformer (CBF) or tapped delay line (TDL) beamformer is designed to use prior knowledge to bring the desired signal to broadside. A block diagram of the broadband CBF is shown in Fig. 3. Prior information about the direction-of-arrival (DoA)
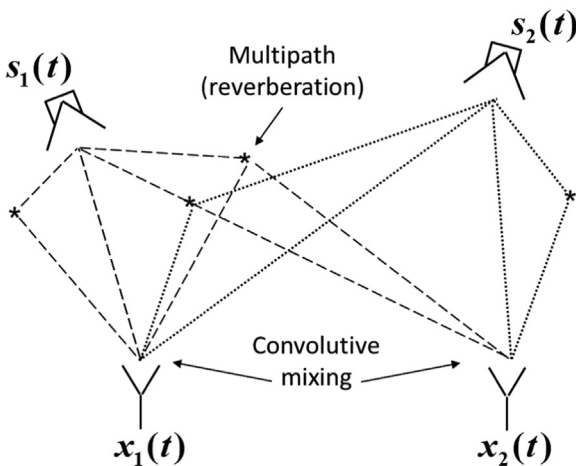

Fig. 2. Block diagram representation of the convolutive mixing model.

of the desired signal and the sensor array is used to specify an estimate of the required pre-steering for the desired signal.

The pre-steering can be expressed as a polynomial vector, $\hat{\mathbf{a}}_s(z)$, and is an estimate of the true pre-steering polynomial vector. The required pre-steering can be found by computing the paraconjugate of the sth column vector in $\mathbf{A}(z)$ of (2), i.e., $\tilde{\mathbf{a}}_s(z)$. The vector $\hat{\mathbf{a}}_s(z)$ describes the necessary filters for bringing sensor contributions due to the desired signal onto broadside. The action of $\hat{\mathbf{a}}_s(z)$ is to form a beam toward the direction of the desired signal. The pre-steered signals are given by

$$\mathbf{v}[t] = \widehat{\mathbf{A}}[t] * \mathbf{x}[t], \tag{12}$$

where $\widehat{\mathbf{A}}[t] = \mathrm{diag}\{\hat{\mathbf{a}}_s[t]\} \in \mathbb{C}^{p \times p}$ and $\hat{\mathbf{a}}_s[t] \circ\!\!-\!\!\bullet \hat{\mathbf{a}}_s(z)$.

The sidelobes of the broadband CBF are fixed relative to the sensor array, however the location of any unwanted signal is not predictable beforehand, and will differ depending on the scenario. For this reason, it is necessary to use a beamformer that will adapt based on the characteristics of any unwanted signals it must mitigate.

In addition to the desired signal, measurements made at the array will, in general, contain other forms of interferences, such as reverberation (reflections from stationary scatterers at various locations) and jamming signals, both direct-path and scattered. Since the lengths of the paths that these signals have to travel differ significantly, and because they differ from element to element of the sensor array, it is impossible to characterise the propagation of the signals by a phase and amplitude change. Consequently, adaptive broadband processing techniques are employed to mitigate these interferences.

3.2. PEVD based broadband BSS

The PCA can perform most of the signal separation if the total power of the desired signal across all the channels differs significantly from the unwanted signals. In the same way, broadband BSS is possible using just a PEVD stage provided the spectra of the signals are different [42,43,46,53]. An estimate of the desired signal is obtained by projecting the mixed signals onto the estimated broadband signal subspace.

Two important features of the SBR2 and SMD algorithms are their very strong tendency to produce signals that satisfy spectral majorisation and their ability to perform power compaction, concentrating as much power into as few channels as possible [26]. These properties enable it to be used for estimating broadband signal and noise subspaces, i.e., broadband subspace decomposition.

Now suppose that the PSD of the desired signal is very different from that of the interference signal. Then the approximately diagonalised CSD matrix in (10) and (11) can be partitioned as

$$\widehat{\mathbf{D}}(z) = \mathrm{diag}\{d_1(z), d_2(z), \mathbf{N}(z)\}, \tag{13}$$

where $d_1(z)$ and $d_1(z)$ tend to be related to the strongest and second strongest source signals, respectively, and $\mathbf{N}(z) = \mathrm{diag}\{d_3(z), \dots d_p(z)\}$ is associated with the sources of noise. This constitutes broadband subspace decomposition; a block diagram representation of this procedure is provided in Fig. 4.

The polynomial eigenvectors of $\widehat{\mathbf{R}}(z)$ in (9) constitute the rows of $\mathbf{H}(z)$ which span $\mathbf{x}[t]$. It is usually assumed that the three subspaces relating to $d_1(z)$, $d_2(z)$ and $\mathbf{N}(z)$ are orthogonal [4,12,41]. Estimation of the source signal is then achieved by orthonormal projection of the data onto the subspace associated with the desired signal, thus

$$\hat{\mathbf{s}}[t] = \mathbf{H}^{\mathrm{H}}[-t] * \mathbf{B} * \mathbf{v}[t], \tag{14}$$

where $\mathbf{B}$ is termed a *blocking matrix* [41,46], which is designed to *block* the contributions from the interference signal. For example, let $d_1(z)$ correspond to the source signal and $d_2(z)$ an interference signal. Then the required projection is given by

$$\mathbf{B} = \mathrm{diag}\{1, \ \mathbf{0}\}, \tag{15}$$

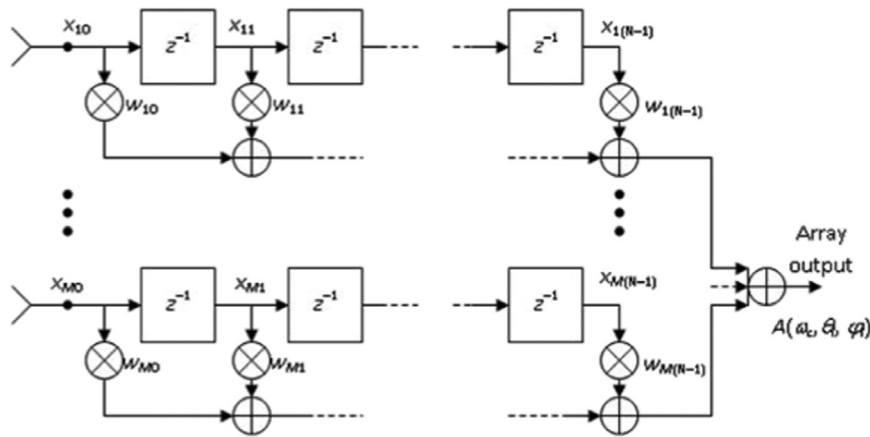where $\mathbf{0}$ is a $1 \times p$ vector of zeros. On the other hand, if the desired

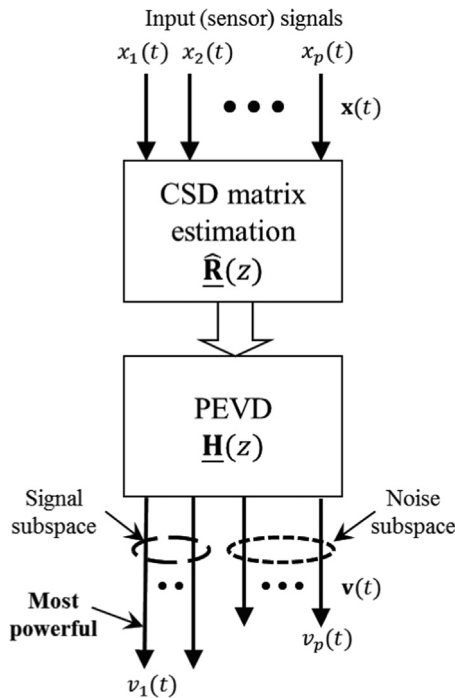**Fig. 3.** Block diagram of the broadband CBF – tapped-delay line beamformer.

Fig. 4. Flowchart of the power-based broadband BSS using PEVD.

signal is very weak compared to the interference, which is often the case for many practical problems, then a more appropriate blocking matrix is

$$\mathbf{B} = \text{diag}\{0, 1, \mathbf{0}\}.$$ (16)

The operation in (14) can be viewed as being analogous to the PCA stage in BSS [1], and thus performing second-order broadband BSS on convolutively mixed signals. Note, however, that it does not perform unmixing in the conventional sense of compensating for the mixing imposed by the mixing matrix $\mathbf{A}[\tau]$ in (2). Instead, it represents separation of the broadband signals from noise, such that the noise power in $\hat{\mathbf{s}}[t]$ is less than that in $\mathbf{x}[t]$ of (2). The procedure outlined here constitutes PEVD-based broadband BSS.

There are a number of applications where PEVD-based broadband BSS can be employed. In the following we consider its application to known problems in sonar detection and radar clutter mitigation.

3.3. PEVD based broadband adaptive beamforming

Application of a broadband adaptive beamformer (ABF) to the problem outlined in Section 3.1 can yield better performance. The ABF

can modify the directivity of the sensor array such that the target return is detected, and interferences and noise are suppressed.

As we have already discussed, the PEVD-based broadband BSS system in Fig. 4 can be used as part of an ABF system with the aim of mitigating interference and noise. A possible PEVD-based ABF is shown in Fig. 5. The PEVD-based broadband ABF comprises three stages:

1. *Interference mitigation*: The PEVD-based broadband BSS described above is applied to suppress the effects due to interferences and noise. Estimates of the broadband signal subspace (signal plus noise subspace) and the noise subspace (interference plus noise subspace) of the input signals are obtained. Projection of the sensor signals onto the estimated broadband signal subspace results in a significant reduction of energy due to the interference. The output signals from this process are 'cleaned' versions of the sensor signals.
2. *Matched filtering*: A receive filter that is matched to the desired signal is employed in order to further enhance the desired signal
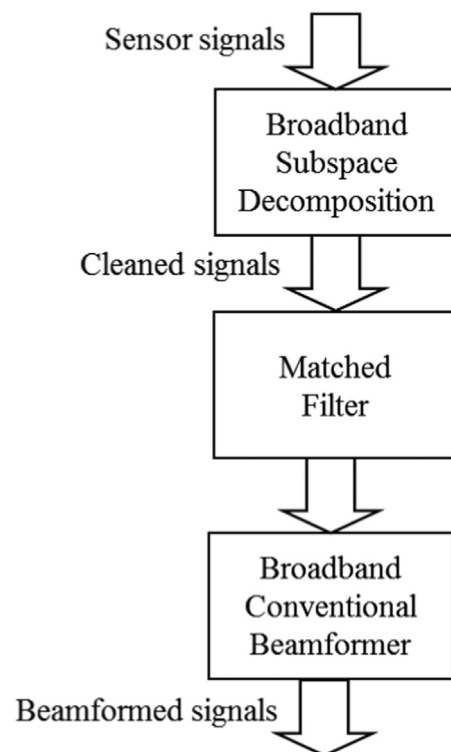

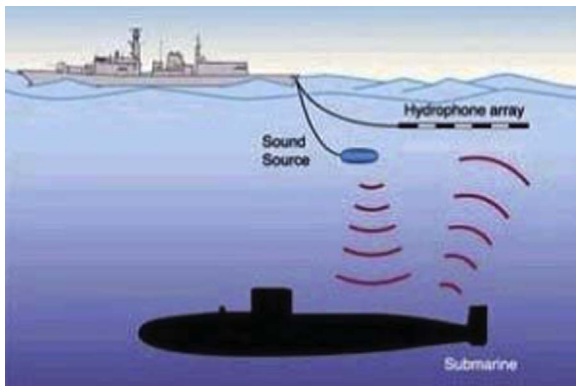**Fig. 5.** Block diagram of a PEVD-based broadband ABF.

Fig. 6. Example of sonar detection.

[54]. For example, in underwater acoustics, a broadband pulsed chirp signal is usually used, so in this case the receive filter is chosen such that it is matched to the transmitted chirp signal [55].

3. *Broadband conventional beamforming*: The output signals from the matched filter are likely to be spread over a wide frequency bandwidth. A pre-steering network is required to focus the phased array beam towards the direction of the desired signal. This can be achieved with the broadband CBF of Fig. 3.

3.4. Example problem I – underwater acoustics

Consider the scenario where a submarine is to be located using a towed array, as depicted in Fig. 6. The desired signal received by a passive array is a reflection from the target of the acoustic source signal transmitted from the towed active array. The reflected signal is a Doppler-shifted version of the source signal. The passive array also receives different time-delayed and attenuated versions of the source signal from different paths due to a reverberant (multipath) environment. This is usually in the presence of a strong broadband (jamming) signal produced by the submarine for concealment purposes; this signal may also be received from different paths. The objective then is to determine the range and bearing of the target in this severe environment given measurements from the passive array.

The propagation of the signal sources to the passive array sensors may be represented in the form of (2). The polynomial mixing matrix $A(z)$ describes the convolutive nature of the channel, as well as encoding the contributions of the source signal to each sensor.

In order to test the PEVD-based broadband ABF described in Section 3.3, we have performed some computer simulations using real trials data gathered from a towed array of p=40 hydrophones. The transmitted signal was a pulsed linear period modulated (LPM) signal with a pulse length of 0.25 s and a pulse repetition interval (PRI) of 15 s. For each PRI's worth of data a power response (range-bearing intensity map) of the beamformer was produced. The data is for the case where a broadband source was used and a continuous-wave (CW) jamming signal was present. Note that, typically, there were two (man-made) sources, i.e., q=2: one corresponding to the pulsed LPM and the other related to the CW tone. However, there were sections of data where the jammer was switched off, in which case the transmitted LPM signal was the only artificial source.

In Fig. 7(a), we show responses of the broadband CBF applied with 12 uniformly spaced taps. Each plot is of range versus bearing obtained by processing the data from a single PRI. From the response of the broadband CBF we see that it is ineffective at localizing the target, especially when a broadband jamming signal is present (right). The jamming signal appears at a single bearing (left hand side plot), but is spread over a large bandwidth, thus hiding the target return. The striation is due to leakage through the sidelobes of the broadband CBF response as the beam is scanned through azimuth.

The performance of the PEVD-based broadband ABF when applied to the aforementioned sonar problem (Fig. 6) was evaluated by computer simulation and some results are presented here. In Fig. 7(b), we show the range-bearing intensity map that results from processing the data from a single PRI with the PEVD-based algorithm. Here the PEVD was obtained using the SBR2 algorithm. Also included in the figure is the response of an IFB approach [56] in Fig. 7(c).

A striking result is that the effects caused by the jamming signal and reverberation are considerably attenuated with both the PEVD-based broadband ABF and the IFB approach for the problem considered. For the case where a jamming signal is present (right hand plots), the highest intensity points on the range-bearing maps correspond to the target. For this data set, the PEVD-based broadband ABF method appears to have suppressed the effects of the jamming signal and the reverberation slightly more than the IFB approach. Interestingly, in the case where there is no jamming signal, the target appears clearer for the plots generated using the PEVD-based broadband ABF compared to the IFB method. This is because PEVD-based broadband ABF is able to mitigate the effects due to the reverberation slightly better than the IFB approach.

It has been shown that the effects due to the reverberation may be further attenuated by re-application of the PEVD-based broadband BSS stage in Fig. 4 to the cleaned sensor signals.

3.5. Example problem II – radar clutter suppression

In Fig. 8, an important example of the radar clutter suppression problem is illustrated. Simulation data was generated for this scenario. A moving radar device carrying an antenna some distance above a terrain surface is used to detect an airborne target. The radar antenna is both a transmitter and a receiver oriented forward towards the direction of travel. Regular successive pulse transmissions are made illuminating the area of terrain bounded by the antenna beam. However, the rough terrain surface within the beam scatters the pulse energy, a proportion of which is received back at the antenna after a time delay. The scattered return energy is termed clutter or backscatter.

The aim is to accurately estimate the DoA and Doppler frequency of the target in the presence of strong and dispersive backscatter from the ground.

To this end, we applied the PEVD-based broadband ABF described in Section 3.3 to simulated data, employing SMD to achieve the factorisation in (10).

The role of the broadband beamformer is to adaptively suppress the radar clutter with little or no prior knowledge of the target signal or the clutter. In this light, it may be viewed as performing (second-order) BSS of broadband (convolutively mixed) signals. An estimate of the DoA and Doppler frequency of the target is then obtained with the application of a broadband CBF.

Our simulations were for three different scenarios each with a target in the presence of clutter and additive white Gaussian noise; the signal-to-noise ratio (SNR) of the target return in all of the datasets was 0 dB. The target DoA is from an azimuth bearing of +16.7° and an elevation angle of −3.8°. The datasets correspond to the following three simulated scenarios:

1. The target return is clear of the clutter in terms of Doppler shift at a higher Doppler frequency (~60 kHz) than the clutter.
2. The target return is in the sidelobe clutter at a lower Doppler frequency than the clutter at ~46 kHz.
3. The target return is in the mainbeam clutter with the same Doppler frequency as the clutter, which is ~54 kHz.

The simulated data is for a moving radar antenna with a 37 element irregular array operating in a high pulse repetition frequency (PRF) mode. The PRF=263.8 kHz (2638 pulses) and there are four range gates. For all datasets, the same clutter signal was used and the SNR of
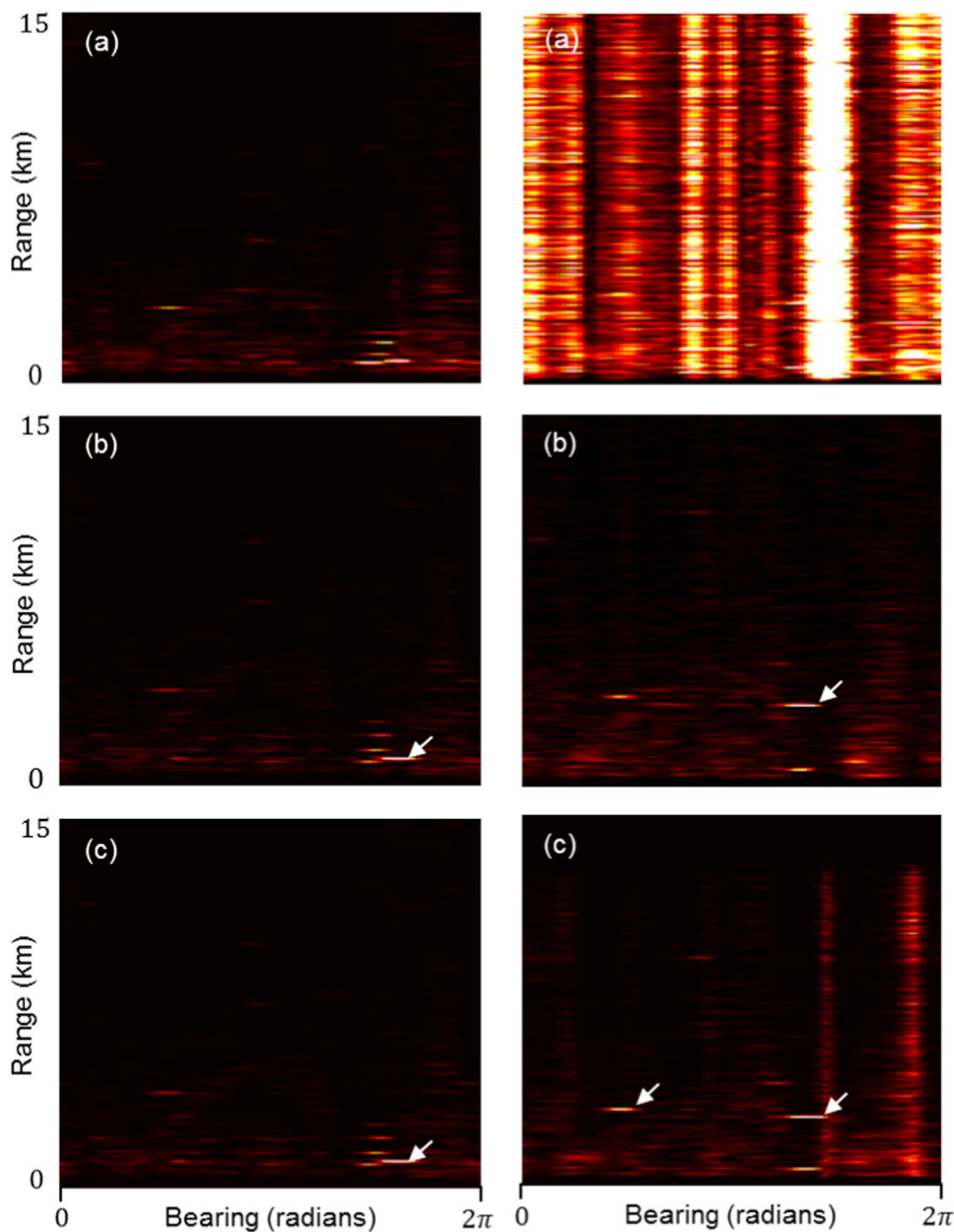
Fig. 7. Range-bearing plots for the (a) broadband CBF, (b) PEVD-based broadband ABF and (c) IFB approach applied to data with reverberation present and (left) no jamming signal and (right) with a strong jamming signal present.
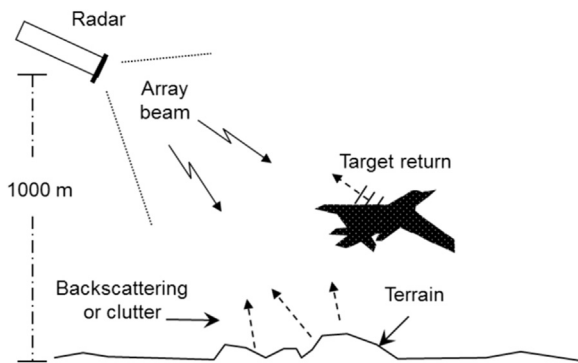

Fig. 8. Example of radar detection.

the clutter was much greater than that of the target return. The target and clutter models used to produce the synthetic data are realistic, detail for which is beyond the scope of this paper.

In a practical radar system, the range of the target is tracked over time, therefore, the range gate that contains the target return is known a priori. The data from this range gate is collected for processing only. The attitude and height of the moving radar are unknown and its range to the target is also unknown.

In Figs. 9–11, graphs of azimuth versus Doppler frequency are shown, which are referred to as angle-Doppler, or bearing-Doppler, maps. For each figure, three angle-Doppler maps are shown; each is for a different elevation angle. The bar to the right of each plot relates the intensity of the returns to the colours used in the plot; the colour red signifies a strong return, whereas blue indicates a weak return. The graphs shown are from images that have been decimated by ten (in the frequency domain) and concentrated in the Doppler range 0–100 kHz.

As observed for the problem in Section 3.4, analysis of the broadband CBF for this problem revealed that, for all three datasets, all of the
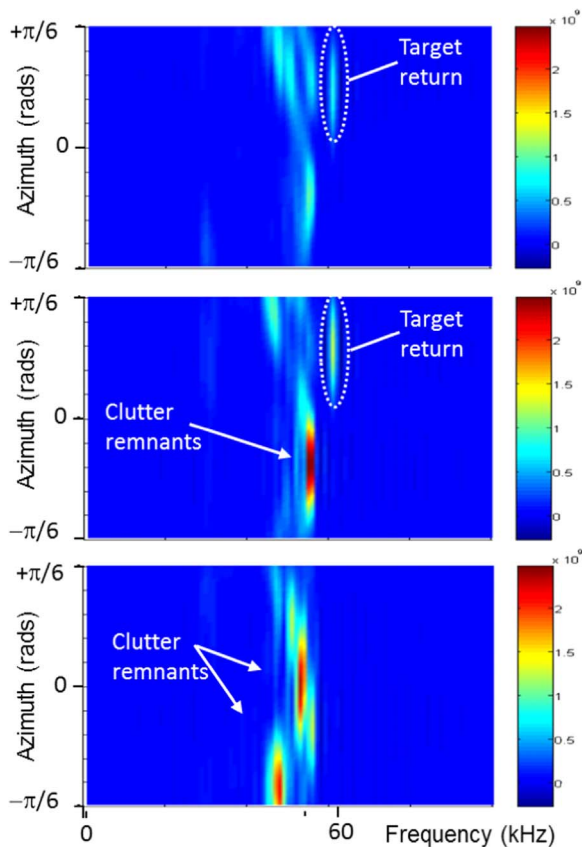
Fig. 9. Angle-Doppler maps related to the output signals from the PEVD-based broadband ABF for elevation angles (a) −15°, (b) 0°, and (c) +15°. The target can be correctly identified at a higher Doppler frequency than the clutter and at boresite elevation; some target return energy is also apparent at negative elevation angles. (For interpretation of the references to colour in this figure, the reader is referred to the web version of this paper.)
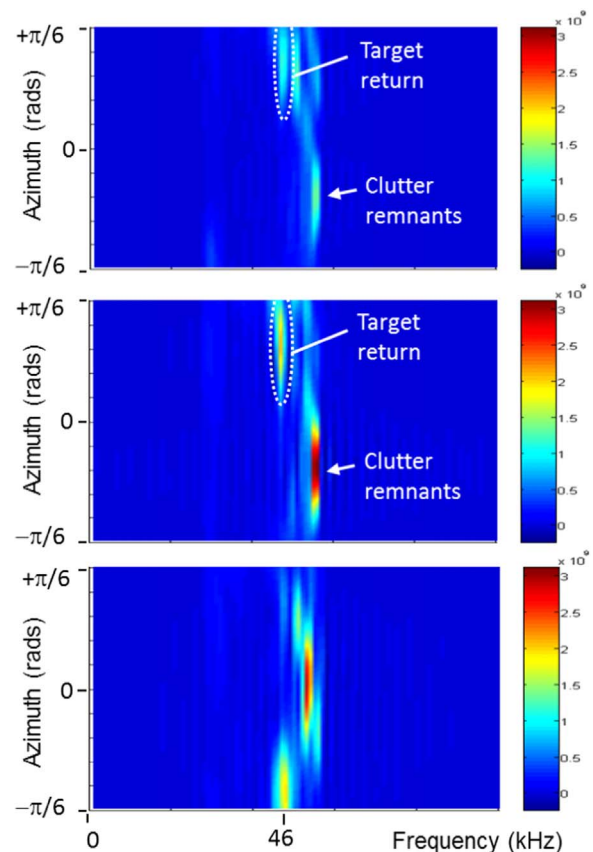

Fig. 10. Angle-Doppler maps related to the output signals from the PEVD-based broadband ABF for elevation angles (a) −15°, (b) 0°, and (c) +15°. Target can be correctly identified in the sidelobe clutter (for negative elevation angles) at a lower Doppler frequency than the clutter. (For interpretation of the references to colour in this figure, the reader is referred to the web version of this paper.)

apparent power was due to backscatter from the ground, the maximum of which was 10^{11}. These results are not shown here.

The power response of the proposed PEVD-based broadband ABF to the input sensor signals, for all three data-set types, was analysed. In graphs (a), (b) and (c) of the figure, we show bearing-Doppler maps for elevation angles (a) −15°, (b) 0° (boresight), and (c) +15°, respectively.

For Fig. 9 it can be deduced that the algorithm has suppressed most of the clutter energy. In particular, notice the reduction in clutter energy at ~50 kHz for an azimuth and elevation angle of, respectively, ~7° and 0° (i.e., boresight); in general, a reduction in clutter power of ~20 dB was achieved. With our prior knowledge of the location of the target, it is easy to see whether the algorithm has been able to extract the target return. We observe that there is a concentration of energy at a Doppler frequency of 60 kHz that coincides with the target azimuth and elevation angles of +16.7° and −3.8°, respectively. This cannot be energy due to backscatter since clutter does not exist in this azimuth-elevation plane for the given Doppler frequency. Therefore, we may deduce from this that the energy concentration is related to the target echo.

A similar level of success has been obtained after processing dataset type (2) – see Fig. 10. In Fig. 11, we show the results for the most difficult simulated scenario (3) (a target in the presence of mainbeam clutter). Here, there is very little or no energy related to the target return, that is, the proposed algorithm cannot distinguish the target echo from the backscatter.

Note that in situations where no prior knowledge of the target location is available, it would be difficult to say with any certainty that the observed target return in Figs. 9 and 10 is the target, since there is still a great deal of clutter power that the algorithm has failed to

remove. However, knowledge about the target's speed is usually available, and so assumptions regarding the required Doppler can be made, which would improve target DoA estimates.

It has to be said that it was never expected that the proposed method would remove the clutter completely since it is operating blindly. At this stage, our PEVD-based broadband ABF is considered as a possible pre-processing stage to post-Doppler space–time adaptive processing.

In conclusion, we can say that in some cases the proposed technique can provide a good level of clutter suppression. However, the target echo cannot be identified with any degree of certainty because our results contain a significant amount of clutter residue. Further processing is required in order to achieve accurate localisation of the target. A possible idea for future work would be to investigate the performance of the PEVD-based broadband ABF with Doppler filtering: the isolation of the Doppler bin of interest before narrowband beamforming is applied.

4. PEVD based broadband BSS using prior knowledge

Algorithms for BSS typically do not exploit prior information about the desired signal nor do they make assumptions that focus attention on the desired signal. As was demonstrated in Section 3, if the spectra of the source signals are different, then the PEVD carries out most of the separation. One way of incorporating prior knowledge into the PEVD-based BSS method of Section 3.2 is to emphasise the desired signal over the unwanted signals by utilizing prior information about the desired signal.
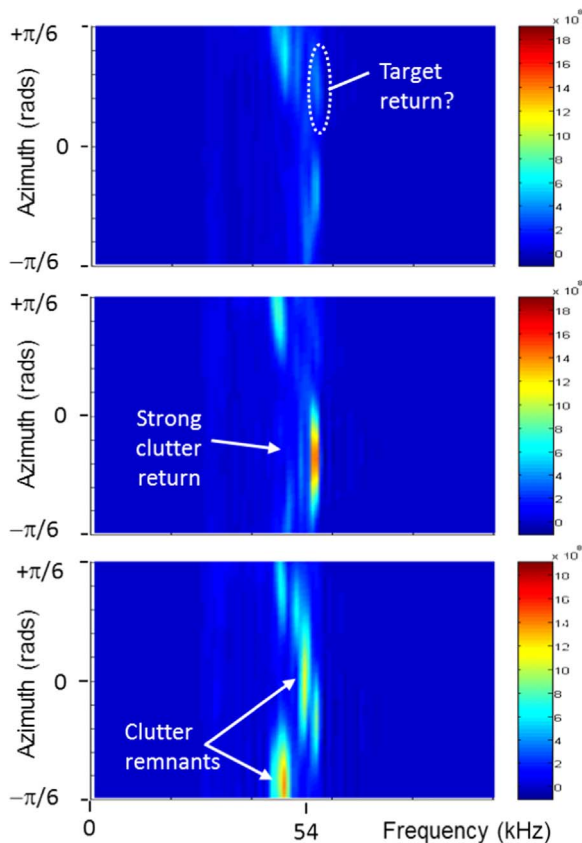
Fig. 11. Angle-Doppler maps related to the output signals from the PEVD-based broadband ABF for elevation angles (a) −15°, (b) 0°, and (c) +15°. There is no clear indication of a target from these results. The target return should be at the same Doppler frequency as the clutter and at a positive azimuth angle. (For interpretation of the references to colour in this figure, the reader is referred to the web version of this paper.)

4.1. Domain-weighted broadband ABF

Different from the scheme shown in Fig. 5, the domain-weighted PEVD (DW-PEVD) [42] exploits knowledge about the desired-signal DoA in order to create a desired signal that is distinct from unwanted (interference) signals. This is achieved by manipulating the desired signal's energy.

With reference to the block diagram of DW-PEVD in Fig. 12, a fixed beamformer, such as the broadband CBF in Section 3.1, is applied as a first stage in order to bring the desired signal to broadside. As with the last stage of the PEVD-based broadband ABF, knowledge about the antenna and the DoA of the desired signal can be used to perform pre-steering for the desired signal.

A generalised sidelobe canceller (GSC) beamformer as in [57] is then applied, which comprises a quiescent vector and a blocking matrix. A suitable quiescent vector designed to pre-steer the signals to the desired DoA is applied, producing a primary channel. The quiescent vector is used to compact power due to the desired signal at broadside into the primary (first) channel; so most of the power related to the desired signal is contained in the primary channel. The columns of the blocking matrix are designed as an orthonormal basis, spanning the quiescent-vector null space, which define a set of $p-1$ auxiliary channels.

The primary-channel signal is scaled by a domain-weighting constant $\mu \in \mathbb{R}$. Provided we have prior knowledge of the DoA of the desired signal, we can 'scale-up' the primary-channel signal with $\mu > 1$. This is the strategy adopted in our experiments to follow – see Section 4.2. Note that the case $\mu=1$ corresponds to the unmodified PEVD with no prior directional information. Also note that the domain-weighting can be a filter, designed to exploit the temporal characteristics of the
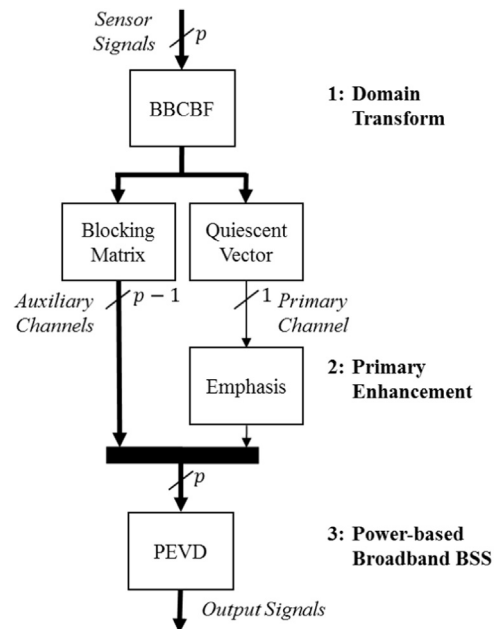
Fig. 12. Block diagram representation of the domain-weighted PEVD method.

desired signal, e.g., a matched filter. However, the performance of such a method may depend to a significant extent on the accuracy of information regarding the acoustic environment.

An iterative PEVD algorithm is then applied to strongly decorrelate a set of signals comprising the auxiliary channel and the emphasised signals. In [42], the SBR2 algorithm was successfully used for this purpose.

Different from existing methods for robust broadband ABF, the DW-PEVD is based on a shift of paradigm away from adaptive noise cancellation toward broadband BSS. The adaptive filtering stage of DW-PEVD is not based on least-squares power minimisation, and so distinct from the GSC, which relies heavily on the availability of correct calibration information. Any signal separation performed by DW-PEVD is done by transferring components of the desired and unwanted signals between channels using a PU transformation, thus conserving the total energy.

The basic philosophy behind DW-PEVD is to provide an extra degree-of-freedom represented by an appropriate choice of emphasis transformation to explore the region between the PEVD, which is entirely blind, and a fixed delay-and-sum beamformer which, being non-adaptive, relies entirely on prior knowledge of the steering vector.

## 4.2. Example problem – sensor arrays

To demonstrate the performance of DW-PEVD, results from numerical simulation of a broadband sensor array problem are presented here. We model a desired signal impinging on a uniform linear array in the presence of an interferer. The array is composed of omnidirectional sensors, where $p=10$, with half-wavelength spacing. The DoA of the desired and interference signals are, respectively, −30° and +20°. An error in array calibration was introduced in the form of a mismatch of +3° in the array response for the desired signal.

The desired signal was modelled as a pulse-shaped, zero-mean, quaternary phase shift keying (QPSK) signal, of which 2000 samples were used. The same model was used to produce the interference signal, except for the application of a different pulse shape. Sensor noise was modelled by zero-mean, unit variance complex Gaussian processes. Both the desired and interference signals had an SNR of 0 dB.

In our experiments, PEVD factorisation was achieved using either the SMD or SBR2C algorithms in [33,31], respectively; the algorithms
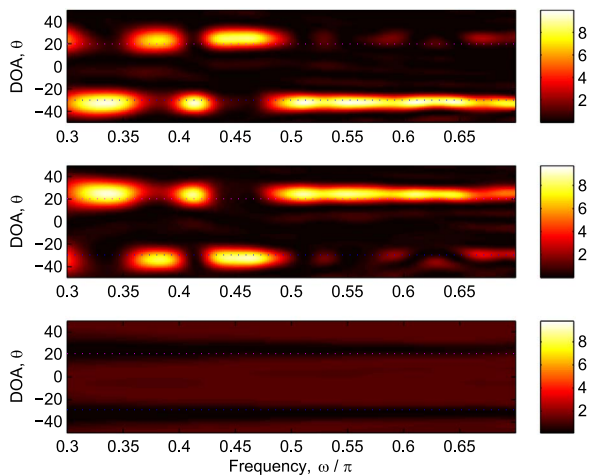
Fig. 13. Beampatterns of the DW-PEVD using SMD, for the case when SNR = INR = 0 dB and for μ=1.
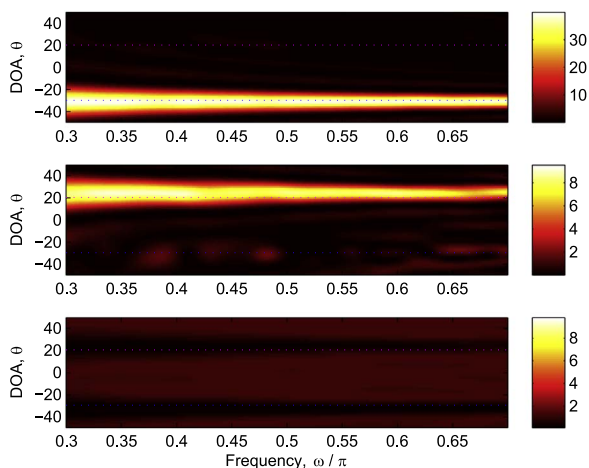
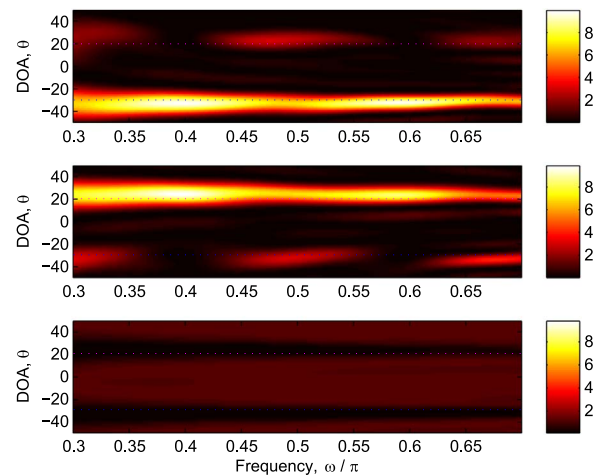**Fig. 14.** Beampatterns of the DW-PEVD using SMD, for the case when SNR = INR = 0 dB and for μ=2.

were allowed to run for 50 iterations. A scalar domain-weighting was applied as the primary enhancement, using only μ=1 or μ=2.

The power response of the overall system in Fig. 12 — convolution of all transformations from sensors to the PEVD — is shown, for three experiments, in Figs. 13–15. Each plot in a figure shows the power of the beam (beampatterns), for different azimuthal angles of arrival and frequency. The top two plots of each figure are the beampatterns for the first and second rows of the transform matrix, respectively, for the whole DW-PEVD system. The third plot is an average beampattern over the rows 3 to p of the matrix. The bar to the right of each plot indicates power level in dBs; white signifies the highest power level, whereas black indicates the lowest power.

Fig. 13 is for the case where no primary enhancement was used, i.e., μ=1. It is clear that the unweighted DW-PEVD cannot perform a good level of signal separation since there is considerable leakage of the look-direction signal into the second channel and the interference signal into the first channel. This is consistent with the theory presented earlier in this section.

In Fig. 14, we show beampatterns for the beamformer with a primary enhancement setting of μ=2 for the same scenario. We can see that the DW-PEVD has designed a first beam which points to the desired signal; the second beam, which is orthogonal to the first, is designed to point in the direction of the interferer. The other beams are orthogonal to the first two beams, as is indicated by very low intensities.

We see that varying the value of μ provides an additional degree-of-

Fig. 15. Beampatterns of the DW-PEVD using SBR2C, for the case when SNR = INR = 0 dB and μ=1.

freedom for achieving good signal separation, and hence interference suppression. Simulation results from assessing the influence of μ have revealed that the DW-PEVD performance has very little dependence on μ at large SNRs. These results are not provided here – the reader is referred to [41] for a thorough characterisation.

In Fig. 15, beampatterns for a beamformer based on the subband-coding variant of SBR2, or the SBR2C algorithm, with a setting of μ=1, for the same scenario, is shown. Notice that even though there is no emphasis on the primary channel, the algorithm does fairly well in separating the two signals, whilst also correctly identifying each signal's DoA.

The improved performance is due to the fact that SBR2C is proportionately equally sensitive to changes in any of the signals [31,41]. While systems with a priori knowledge will usually perform better, the SBR2C-based system is able to recover the signals and their DoAs without this knowledge.

5. Conclusions

The overarching goal of this paper has been to build intuition and insight into the important field of polynomial matrix decompositions and its relevance to broadband BSS while leaving the detail to references.

Sample applications in the areas of broadband BSS and beamforming have been presented along with solutions and new results to three important problems via a polynomial EVD based broadband beamformer and a domain-weighted polynomial EVD. The results have been compared to those of classical broadband methods, which highlights the suitability of the polynomial EVD to the problem of broadband BSS.

References

[1] P. Comon, Independent component analysis, a new concept?, Signal Process. 36 (April (3)) (1994) 287–314.
[2] A. Hyvarinen, J. Karhunen, E. Oja, Independent Component Analysis, John Wiley and Sons, NY, 2001.
[3] G.H. Golub, C.F. Van Loan, Matrix Computations, 3rd edition, John Hopkins University Press, Baltimore, Maryland, 1996.
[4] S. Haykin, Adaptive Filter Theory, 4th edition, Prentice Hall, Englewood Cliffs, NJ, 2002.

[5] J. Bobin, J.-L. Starck, M.J. Fadili, Y. Moudden, Sparsity and morphological diversity in blind source separation, IEEE Trans. Image Process. 16 (November (11)) (2007) 2662–2674.

[6] J. Zhang, H. Zhang, L. Wei, Y.J. Wang, Blind source separation with pattern expression NMF, in: Advances in Neural Networks ISNN 2006, Springer-Verlag, Heidelberg, 2006, vol. 3971, pp. 1159–1164.

[7] A.S. Montcuquet, L. Hervé, F. Navarro, J.M. Dinten, J.I. Mars, Nonnegative matrix factorization: a blind spectra separation method for in vivo fluorescent optical imaging, J. Biomed. Opt. 15 (September (5)) (2010) 056009.

[8] B.M. Abadi, A. Sarrafzadeh, F. Ghaderi, S. Sanei, Semi-blind channel estimation in MIMO communication by tensor factorization, in: IEEE Workshop on Statistical Signal Processing, August 2009, pp. 313–316.

[9] P.P. Vaidyanathan, Theory of optimal orthonormal subband coders, IEEE Trans. Signal Process. 46 (June (6)) (1998) 1528–1543.

[10] P. Smaragdis, Blind separation of convolved mixtures in the frequency domain, Neurocomputing 22 (1998) 21–34.

[11] S. Ikeda, N. Murata, A method of ICA in time–frequency domain, in: Workshop on Independent Component Analysis and Signal Separation, 1999, pp. 365–370.

[12] H. Wang, M. Kaveh, Coherent signal-subspace processing for the detection and estimation of angles of arrival of multiple wide-band sources, IEEE Trans. Acoust. Speech Signal Process. 33 (August (4)) (1985) 823–831.

[13] H. Hung, M. Kaveh, Focussing matrices for coherent signal-subspace processing, IEEE Trans. Acoust. Speech Signal Process. 36 (August (8)) (1988) 1272–1281.

[14] Y. Bucris, I. Cohen, M.A. Doron, Bayesian focusing for coherent wideband beamforming, IEEE Trans. Audio Speech Lang. Process. 20 (May (4)) (2012) 1282–1296.

[15] T. Kailath, Linear Systems, Prentice Hall, Englewood Cliffs, NJ, 1980.

[16] R.H. Lambert, M. Joho, H. Mathis, Polynomial singular values for number of wideband source estimation and principal components analysis, in: Proceedings of International Conference on Independent Component Analysis, 2001, pp. 379–383.

[17] R.H. Lambert, Multichannel blind deconvolution: FIR matrix algebra and separation of multipath mixtures (Ph.D. thesis), University Southern California, LA, 1996.

[18] P.A. Regalia, P. Loubaton, Rational subspace estimation using adaptive lossless filters, IEEE Trans. Signal Process. 40 (October (10)) (1992) 2392–2405.

[19] P.P. Vaidyanathan, Multirate Systems and Filter Banks, Prentice Hall, Englewood Cliffs, 1993.

[20] P. Desarte, B. Macq, D.T.M. Slock, Signal-adapted multiresolution transform for image coding, IEEE Trans. Inf. Theory 38 (March (2)) (1992) 897–904.

[21] P.A. Regalia, D.-Y. Huang, Attainable error bounds in multirate adaptive lossless FIR filters, in: Proceedings of IEEE Conference on Acoustics, Speech, and Signal Processing, 1995, pp. 1460–1463.

[22] P. Moulin, M.K. Mihcak, Theory and design of signal-adapted FIR paraunitary filter banks, IEEE Trans. Signal Process. 46 (April (4)) (1998) 920–929.

[23] B. Xuan, R.I. Bamberger, FIR principal component filter banks, IEEE Trans. Signal Process. 46 (April (4)) (1998) 930–940.

[24] X. Gao, T.Q. Nguyen, G. Strang, On factorization of M-channel paraunitary filterbanks, IEEE Trans. Signal Process. 49 (July (7)) (2001) 1433–1446.

[25] J.G. McWhirter, P.D. Baxter, A novel technique for broadband SVD, in: 12th Annual Workshop Adaptive Sensor Array Processing, MIT Lincoln Labs, Cambridge, MA, 2004.

[26] J.G. McWhirter, P.D. Baxter, T. Cooper, S. Redif, J. Foster, An EVD algorithm for para-Hermitian polynomial matrices, IEEE Trans. Signal Process. 55 (May (5)) (2007) 2158–2169.

[27] A. Tkacenko, P.P. Vaidyanathan, Iterative greedy algorithm for solving the FIR paraunitary approximation problem, IEEE Trans. Signal Process. 54 (January (1)) (2006) 146–160.

[28] A. Tkacenko, Approximate eigenvalue decomposition of para-Hermitian systems through successive FIR paraunitary transformations, in: IEEE International Conference on Acoustics Speech, and Signal Processing, March 2010, pp. 4074–4077.

[29] J.G. McWhirter, An algorithm for polynomial matrix SVD based on generalised Kogbetliantz transformations, in: European Signal Processing Conference, Aalborg, Denmark, 2010, pp. 457–461.

[30] J.A. Foster, J.G. McWhirter, M.R. Davies, J.A. Chambers, An algorithm for calculating the QR and singular value decompositions of polynomial matrices, IEEE Trans. Signal Process. 58 (March (3)) (2010) 1263–1274.

[31] S. Redif, J.G. McWhirter, S. Weiss, Design of FIR paraunitary filter banks for subband coding using a polynomial eigenvalue decomposition, IEEE Trans. Signal Process. 59 (November (11)) (2011) 5253–5264.

[32] S. Redif, S. Weiss, J.G. McWhirter, An approximate polynomial matrix eigenvalue decomposition algorithm for para-Hermitian matrices, in: IEEE 11th International Symposium on Signal Processing and Information Technology, Bilbao, Spain, 2011,

pp. 421–425.

[33] S. Redif, S. Weiss, J.G. McWhirter, Sequential matrix diagonalisation algorithms for polynomial EVD of parahermitian matrices, IEEE Trans. Signal Process. 63 (January (1)) (2015) 81–89.

[34] S. Icart, P. Comon, Some properties of Laurent polynomial matrices, in: 9th IMA Conference on Mathematics in Signal Processing, Birmingham, UK, December 2012.

[35] S. Kasap, S. Redif, Novel field-programmable gate array architecture for computing the eigenvalue decomposition of para-Hermitian polynomial matrices, IEEE Trans. Very Large Scale Integr. Syst. 22 (March (3)) (2014) 522–536.

[36] J. Corr, K. Thomson, S. Weiss, J.G. McWhirter, S. Redif, I.K. Proudler, Multiple shift maximum element sequential matrix diagonalisation for parahermitian matrices, in: IEEE Workshop on Statistical Signal Processing, Gold Coast, Australia, July 2014, pp. 312–315.

[37] Z. Wang, J.G. McWhirter, J. Corr, S. Weiss, Multiple shift second order sequential best rotation algorithm for polynomial matrix EVD, in: IEEE European Signal Processing Conference, Nice, France, August 2015, pp. 844–848.

[38] M. Tohidian, H. Amindavar, A.M. Reza, A DFT-based approximate eigenvalue and singular value decomposition of polynomial matrices, EURASIP J. Adv. Signal Process. 1 (2013) 1–16.

[39] R. Brandt, M. Bengtsson, Wideband MIMO channel diagonalization in the time domain, in: International Symposium on Personal, Indoor and Mobile Radio Communications, 2011, pp. 1914–1918.

[40] J. Corr, K. Thompson, S. Weiss, I.K. Proudler, J.G. McWhirter, Shortening of paraunitary matrices obtained by polynomial eigenvalue decomposition algorithms, in: 5th Conference of the Sensor Signal Processing for Defence, Edinburgh, UK, July 2015.

[41] S. Redif, Polynomial matrix decomposition and paraunitary filter banks (Ph.D. thesis), University of Southampton, 2006.

[42] S. Redif, J.G. McWhirter, P.D. Baxter, T. Cooper, Robust broadband adaptive beamforming via polynomial eigenvalues, in: IEEE/MTS OCEANS'06, Boston, MA, September 2006, pp. 1–6.

[43] S. Redif, U. Fahrioglu, Foetal ECG extraction using broadband signal subspace decomposition, in: IEEE Mediterranean Microwave Symposium, Guzelyurt, Cyprus, 2010. pp. 381–84.

[44] M.A. Alrmah, S. Weiss, S. Lambotharan, An extension of the MUSIC algorithm to broadband scenarios using polynomial eigenvalue decomposition, in: 19th European Signal Processing Conference, Spain, September 2011, pp. 629–633.

[45] M. Alrmah, S. Weiss, S. Redif, S. Lambotharan, J.G. McWhirter, M. Kaveh, Angle of arrival estimation for broadband signals: a comparison, in: IET Intelligent Signal Processing Conference, London, UK, December 2013.

[46] S. Redif, Fetal electrocardiogram estimation using polynomial eigenvalue decom-position, Turk. J. Electr. Eng. Comput. Sci. 24 (August (4)) (2014) 2483–2497.

[47] S. Weiss, S. Bendoukha, A. Alzin, F. Coutts, I. Proudler, J. Chambers, MVDR broadband beamforming using polynomial matrix techniques, in: 23rd European Signal Processing Conference, Nice, France, September 2015, pp. 844–848.

[48] S. Weiss, S. Redif, T. Cooper, C. Liu, P. Baxter, J.G. McWhirter, Paraunitary oversampled filter bank design for channel coding, EURASIP J. Appl. Signal Process 2006 (2006) 1–10. http://dx.doi.org/10.1155/ASP/2006/31346 ID 31346.

[49] J. Foster, J. McWhirter, S. Lambotharan, I. Proudler, M. Davies, J. Chambers, Polynomial matrix QR decomposition for the decoding of frequency selective multiple-input multiple-output communication channels, IET Signal Process. 6 (September (7)) (2012) 704–712.

[50] Z. Wang, J.G. McWhirter, S. Weiss, Multichannel spectral factorization algorithm using polynomial matrix eigenvalue decomposition, in: Asilomar Conference on Signals, Systems, and Computers, 2015.

[51] S. Redif, S. Kasap, Novel reconfigurable hardware architecture for polynomial matrix multiplications, IEEE Trans. Very Large Scale Integr. Syst. 23 (March (3)) (2015) 454–465.

[52] P.D. Baxter, J.G. McWhirter, Robust adaptive beamforming based on domain weighted PCA, in: 13th European Signal Processing Conference, Antalya, Turkey, 2005.

[53] G.D. Clifford, Singularvalue decomposition and independent component analysis for blind signal separation, Bio Signal Image Process. 44 (6) (2005) 489–499.

[54] H.L. Van Trees, Detection, Estimation and Modulation Theory, Wiley & Sons Inc., USA, 1968 ISBNs: 0-471-09517-6.

[55] J.-P. Hermand, W.I. Roderick, Acoustic model-based matched filter processing for fading time-dispersive ocean channels: theory and experiment, IEEE Trans. Ocean. Eng. 18 (October (4)) (1993) 447–465.

[56] R. Klemm, Space–Time Adaptive Processing Principles and Applications, Series 9, IEE Radar, Sonar, Navigation and Avionics, London, UK, 1998.

[57] L.J. Griffiths, C.W. Jim, An alternative approach to linearly constrained adaptive beamforming, IEEE Trans. Antennas Propag. 30 (January (1)) (1982) 27–34.